Controlled deposition of 2D-confined Pd or Ir nano-islands on Au(1 1 1) following Cu UPD, and their HER activity

Daniel Ohm, Katrin F. Domke *

Electrochemical Surface Science Group, Max Planck Institute for Polymer Research, Ackermannweg 10, 55128 Mainz, Germany

ARTICLE INFO

ABSTRACT

Platinum-group metals are very efficient electro-catalysts for a variety of important energy conversion reactions, *e.g.* for oxygen or hydrogen evolution, but are scarce and expensive. One way to improve the catalyst mass activity and thus to lower costs is to increase the number of active sites per surface area, for example, by nano-confining the catalyst. Here, we systematically investigate Pd and Ir monoatomic island formation based on Cu underpotential deposition and subsequent metal displacement on Au(1 1 1). We find that island size and dispersion can be controlled by Cu deposition potential and duration. We examine how the hydrogen evolution reaction on the as-prepared 2D Pd or Ir islands on Au(1 1 1) can be tuned by selectively tuning island size and inter-island distance on the nanoscale. The HER charge density of the islands was found to show a maximum for intermediate deposition times.

1. Introduction

Platinum group metals (PGMs) are well established catalysts for important electrochemical energy conversion reactions, such as, for example, the hydrogen or oxygen evolution or reduction reactions (HER/HRR; OER/ORR) [1–4]. Bulk PGM electrodes, however, are scarce and very expensive [5], and a reduction of material use of and costs for electrocatalysts is of paramount interest. One key indicator for improved catalysts is the mass activity that is defined by the specific catalytic activity of a material for a given (electro)catalytic reaction normalized to the surface area, and, in turn, normalized to the amount (mass) of a catalytically active material [6]. An increase in mass activity results in cheaper electrode catalyst material, and, therefore, renders energy conversion devices such as fuel cells or electrolysers more cost efficient.

One straightforward approach to reducing catalytic material is to fabricate catalyst nano-islands. For PMG metals, Pd submonolayers deposited on Au are one of the most widely studied systems [7].

Various ways for Pd submonolayer deposition from solution onto Au have been reported. Amongst other, Pd underpotential deposition is widely employed. For example, fabrication of Pd islands on Au was presented by Kibler, Kolb and co-workers who found that Pd overlayers on Au(1 1 1) grow to irregularly shaped triangles during underpotential deposition from Pd sulfate salt before more layers are formed during overpotential [8,9]. This deposition method was further

employed to systematically investigate step effects on HER [10]. On the other hand, also spontaneous deposition of Pd from salts can be employed to form submonolayers on Au [11]. Interestingly, it has been demonstrated that specifics like applied potential and the presence of a reducing hydrogen atmosphere during Pd deposition play an important role for the overall catalytic activity of the resulting Pd/Au sample [12].

Distinct reactivities of differently prepared Pd/Au samples can often be ascribed to the amount of deposited Pd. Pandelov and Stimming showed that Pd adlayers down to sub-monolayer islands of diameters of <5 nm on Au enhance the rate of hydrogen reduction by up to two orders of magnitude for partial coverages down to 0.035 ML, where the catalytic activity increases with decreasing number of Pd layers [13]. The effect of Pd surface coverage on Au(1 1 1) for HER was theoretically explored by Nørskov and co-workers, highlighting the importance of rim sites for the catalyst activity [14].

Here, we systematically investigate an alternative route toward 2D Pd or Ir nano-islands fabrication on Au(1 1 1) based on Cu underpotential deposition (UPD) and subsequent galvanic displacement, similar to the monolayer deposition described earlier by Adžić and co-workers [15].

To obtain a regular and controllable distribution of islands, we employ a reaction pathway in which mono-atomically high Pd and Ir islands of 5–40 nm diameter are obtained from galvanic displacement of Cu islands on Au(1 1 1) that were previously formed by Cu UPD
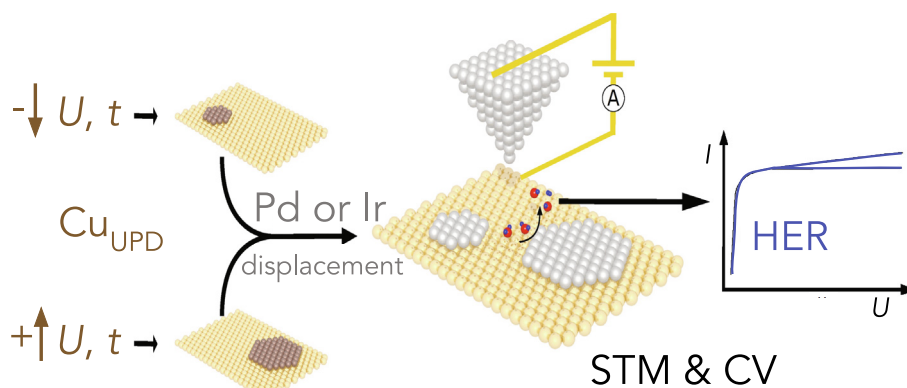
Fig. 1. Schematic depiction of the controlled Pd or Ir island fabrication on Au(111) and subsequent evaluation of the HER activity. U: electrode potential; t: deposition time; Cu UPD: Cu underpotential deposition; STM: scanning tunnelling microscopy; CV: cyclic voltammetry.

(Fig. 1). Cu UPD is a well-established technique that allows to deposit Cu sub-monolayers at underpotential on bulk metal electrodes [16–20]. We show that the Pd or Ir island size and inter-island distance can be selectively tuned by the choice of Cu UPD potential and duration. The resulting Au/Pd or Au/Ir catalyst surfaces are evaluated with respect to their HER activity.

The primary advantage of the proposed two-step method compared to other deposition approaches is the separation of the island formation via Cu UPD and the subsequent deposition of the target metal via galvanic displacement. The proposed route allows to control the island deposition through the well-established Cu UPD process and then to replace the Cu islands by, in principle, any other more noble metal without the need to develop suitable deposition methods for each metal.

2. Experimental section

2.1. Chemicals and glassware

All solutions were prepared with Milli-Q water (Millipore, 18.2 MΩ, 3 ppb TOC) and 96% H_2SO_4 (Suprapur, Merck). The electrolyte for Cu UPD was prepared from copper(II) pentahydrate (Merck). Palladium chloride (99%, Merck) and hydrogen hexachloroiridate(IV) hydrate (99.8% trace metals basis, Merck) were used as solutions in HCl for the galvanic metal displacement. Before each experiment, the working solution was purged with Ar (6.0 Westfalen) for 15 min. During the experiment, an Ar flow was kept above the solution. Glassware and Teflon parts for electrochemical measurements were cleaned by boiling them in 40% HNO_3 followed by three cycles of rinsing with and boiling in Milli-Q water.

2.2. Gold thin films

Au thin films were prepared by thermal evaporation of Au beads (4 N) onto cleaned N-LaSF9 glass slides covered with a 5–10 nm thick chrome layer. The evaporation was performed using an Edwards FL 400 evaporator at a pressure of $< 5 \times 10^{-6}$ mbar and an evaporation rate of 0.05 nm s^{-1} to reach a gold thickness of 150 nm–200 nm.

Au/Cr/glass slides were cleaned by immersing them for 2 min in 40% nitric acid at room temperature and subsequent rinsing with Milli-Q water. The slides were flame-annealed to red glowing color in the oxidation zone of a Bunsen burner flame for 5 min. It was taken care that the Au layer was not damaged during the annealing by letting the surface cool down outside the flame after it started glowing. This

procedure was repeated multiple times during the 5 min overall annealing time. After the annealing, the sample was thoroughly rinsed with Milli-Q water. Directly after annealing and rinsing the sample, a gold wire (Merck, diameter: 0.5 mm, 99.997% trace metal basis) for contacting the sample was attached to the surface using Teflon tape (Hightech-flon, thickness: 0.13 mm, hole diameter: 6 mm). The Teflon tape was cut so that it juts out by around 1–2 mm over the sample boundaries, far enough that the two sides of the tape stick together. A hole with a diameter of 6 mm was stamped into the tape to expose a well-defined surface area to the electrolyte solution. The Au samples were used in the electrochemical cell directly after preparation.

2.3. Cyclic voltammetry

Cyclic voltammetry (CV) measurements were performed using a Metrohm Autolab PGSTAT30 Potentiostat with a Metrohm Autolab Differential Electrometer Amplifier attached. NOVA (Version 2.1, Windows 7) was used as software for the electrochemical measurements. For the CV experiments, a three-electrode setup with a Au-wire counter electrode, a H_2-loaded Pd reference electrode and the Au-sample working electrode were used. The Pd wire (0.5 mm diameter, MaTecK, 99.95% metals basis) was filled with H_2 by immersing it into 0.1 M H_2SO_4 and applying 5–10 V between the Pd wire and the Au counter electrode until the hydrogen evolution corresponded roughly to the oxygen gas bubble evolution. The potentials were converted and are reported in this study versus the standard hydrogen electrode (SHE). The electrochemical measurements were performed in self-designed glass cells with 50 mL cell volume. 0.1 M H_2SO_4 was used as electrolyte for all reported experiments in which Pd or Ir island samples were used.

2.4. Cu underpotential deposition

A freshly prepared 1 mM solution of $CuSO_4$ in 0.1 M H_2SO_4 was used as electrolyte for Cu UPD. All Cu UPD experiments were performed according to the same experimental procedure with varying the deposition potential and/or deposition time as described in the following. After bubbling Ar through the electrolyte for 10 min, the electrolyte solution was blanketed with Ar. Cu UPD was performed by applying a start potential of 0.5 V vs Cu/Cu^{2+} to the electrode and holding it for 15 s to let the system reach equilibrium. Then the potential was set to the target potential of 0.12 V or 0.15 V vs Cu/Cu^{2+} and held for the indicated duration before switching to open circuit potential. The cell was shut off, and the working electrode was removed and briefly rinsed in Milli-Q water.

2.5. PGM galvanic displacement

10 mM aqueous solutions of palladium(II) chloride or hydrogen hexachloroiridate(IV) hydrate were used for galvanic metal displacement. After Cu UPD, the samples were rinsed in Milli-Q water and directly immersed into the metal salt solution (either Pd or Ir containing) for 10 s and subsequently carefully rinsed with Milli-Q water.

2.6. Tafel plots

Tafel plots were derived from polarization curves in the potential range from −0.2 V to 0.2 V vs SHE recorded at a sweep rate of 25 mV/s versus a H_2-loaded Pd pseudo reference electrode. The linear regime of log|j| vs overpotential was plotted and linearly fitted to obtain the HER onset potential (Tafel constant) and the Tafel slope.

3. Results and discussion

3.1. Pd and Ir island fabrication – the influence of Cu UPD potential and duration

Cu UPD is a very well known process. Former studies have shown that the amount of charge needed to deposit one full monolayer (ML) of Cu onto Au(1 1 1) lies between 0.35 [21] and 0.46 [22] mC/cm². The Cu UPD cyclic voltammogram (CV) shows two sharp adsorption peaks at 550 mV and 370–350 mV vs SHE with a charge ratio of 2:1 (Fig. 2a, inset). At potentials lower than 320 mV, the bulk deposition of Cu starts. Early LEED measurements have shown a $(\sqrt{3} \times \sqrt{3})R30$ structure of the overlayer inbetween the two adsorption peaks [23]. It is also known that the presence of anions plays a role in Cu UPD. CV measurements in perchloric acid showed only one broad deposition peak before bulk deposition starts [24]. Cu UPD nucleation and growth follows a 2D nucleation and growth process limited by a lattice incorporation process (2D-LI). Nucleation rate and number density of active sites of the Cu UPD are both potential dependent [25]. While the Cu UPD process has been extensively studied for years [21–24,26], a systematic approach to prepare sub-monolayer islands of controlled size and surface dispersion is still lacking. Fig. 2a shows a typical current/time (I/t) trace recorded during Cu UPD at 0.44 V vs SHE and the CV of the Cu deposition and dissolution processes in the cathodic and anodic scans, respectively (Fig. 2a, inset). The exponential decay of the current density with time indicates that the deposition process is not merely diffusion controlled [27]. For a deposition process following nucleation and growth law, the current density would go through a minimum followed by a local maximum [28].

Fig. 2b displays the correlation between Cu deposition duration and resulting Cu surface coverage for two different deposition potentials of 0.44 V (gray) and 0.47 V (black) vs SHE, respectively. The deposition potentials were chosen to lie within a potential range where, according to literature, the first third of a ML of Cu is deposited onto the gold surface [29,30]. The results show that the surface coverage as obtained from the CV current depends strongly on both, deposition potential and deposition duration. At 0.47 V vs SHE, the surface coverage increases linearly with short deposition duration of up to 6 s, ranging from 0.24 ML at 3 s to 0.28 ML at 6 s. For deposition durations longer than 6 s, the curve flattens out and reaches 0.32 ML at 16 s deposition duration. For a higher deposition potential of 0.47 V vs SHE, the curve is shifted to slightly longer durations, i.e. the surface coverage at same deposition duration is smaller for higher deposition potentials than for lower potentials. The small difference in deposition potential of 40 mV leads to a notable difference of about 0.04 up to 0.06 ML in surface coverage for the same deposition duration. For a deposition duration of 3 s, the surface coverage at lower potential of 0.44 V vs SHE increases by 25% compared to a higher deposition potential of 0.47 V vs SHE.

The data show that the deposition potential has a larger influence on the resulting Cu surface coverage than the deposition duration. To reach a coverage of more than 0.30 ML up to the maximum coverage of 0.33 ML at a deposition potential of 0.44 V vs SHE, a long deposition duration of more than 10 s is needed, whereas 0.30 ML can be reached after 3 s at lower deposition potentials of 0.44 V vs SHE. This result can be understood in terms of the exponential behaviour of the current density vs time trace during the deposition (Fig. 2a). Apparently, a more negative deposition potential leads to a higher initial current density. With time, the current density decreases exponentially and is only about 25% of the initial one after a deposition duration of 1 s. At later times, the increase in current density levels off. For a deposition potential of 0.47 V vs SHE, the current density after 1 s deposition duration has decreased from initially 492 µA/cm² to 6 µA/cm². As such, the deposition duration >1 s can be employed to fine-tune the amount of Cu deposited onto the Au surface. At longer times of around 10 s (0.44 V vs SHE) to 15 s (0.47 V SHE), the surface coverage approaches the maximum of one third of a full Cu monolayer, as typically expected and achieved for deposition potentials above 0.35 V vs SHE [29,30]. To reach a higher surface coverage than 0.33 ML, a further decrease in deposition potential is required because increasing the deposition time does not lead to higher coverage as can be derived from the CV of Cu UPD on Au(1 1 1) (inset Fig. 2a) [31]. In general, the lower the deposition potential, the faster a surface coverage of 0.33 ML can be reached. Note that rinsing the Cu UPD samples
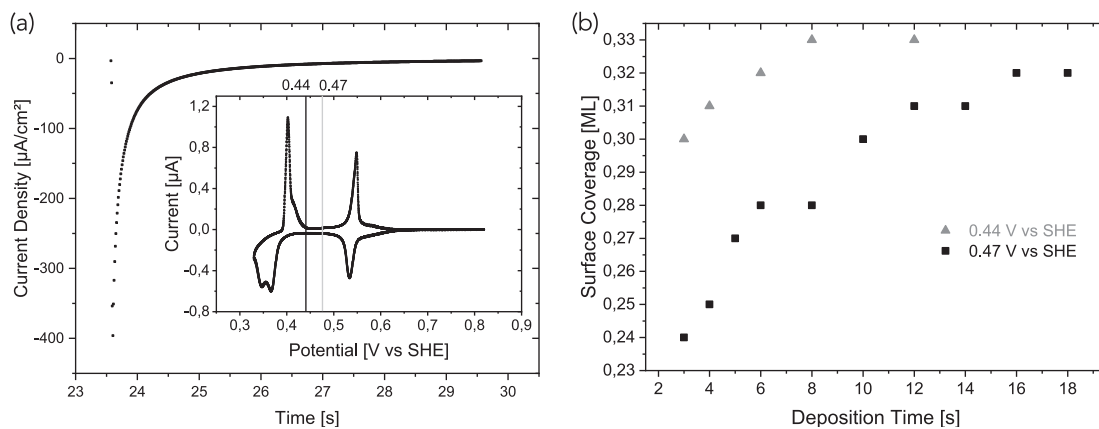
Fig. 2. (a) Current density versus time trace recorded during Cu UPD on Au(1 1 1). Deposition potential: 0.44 V (grey) and 0.47 (black) vs SHE, 6 s deposition time. Prior to deposition, the immersion potential of 0.72 V vs SHE was held for 23.5 s. Inset shows the CV of a Cu UPD. Vertical black and grey lines indicate 0.44 and 0.47 V vs SHE deposition potentials, respectively. (b) Surface coverage as obtained from CV current as a function of deposition duration and deposition potential.

with non-deaerated MilliQ water does not have any effect on the resulting Cu island size and shape according to STM imaging or on the metal displacement OCP (Supplementary Information, Figs. S1–13), ruling out that the sample processing affects the results.

Fig. 3a shows a typical STM image of the surface after Pd displacement. Further STM image examples for clean Au(111), Pd/Au(111) and Ir/Au(111) can be found in Figs. S14–S29. Small, bright islands are discernible on large terraces and at monoatomic step edges of the Au(111) substrate that are mostly of 0.33 nm height, close to the Pd atomic diameter of 0.34 nm. Similar images were obtained for Ir displacement, displaying a slightly larger island height of 0.37 nm as expected for an Ir atomic diameter of 0.36 nm (Fig. S15). The presence of Pd or Ir and the absence of Cu after galvanic displacement was further confirmed by XPS (Figs. S30–S34). For some Pd samples (albeit not for Ir ones), we observe also regions of apparent smaller height of ca. 0.1 nm. We speculate that the flatter islands might be Pd that is partially oxidized [32] under the given sample preparation conditions where air contact cannot be avoided, resulting in a lower tunneling current and thus apparent lower island height.

Note that while the CVs (Fig. 2b) indicate a Cu coverage between 0.24% and 0.33% for all experiments, the coverage data extracted from the STM images (SI Table S1) exhibit a wide range from less than 5% to 65%, thus reaching values much larger than the theoretical maximum of 33%. The large variation in STM coverage values indicates that this value strongly depends on the spot where the STM image was taken and does not capture site-to-site differences in surface coverage that could be significant. While the STM images show a qualitative trend for island size and inter-island spacing, they do not allow us to quantify the efficiency of the metal displacement.

Fig. 3b gives an overview of the correlation of average Pd island diameter as obtained from STM image analysis with the Cu UPD deposition potential and duration. At a deposition potential of 0.44 V vs SHE, the average island diameter increases with increasing deposition duration from 2 nm ± 0.6 nm at 3 s to 3 nm ± 0.5 nm at 6 s. At the higher deposition potential of 0.47 V vs SHE, the average Pd island size increases from 5 nm ± 1 nm at 3 s to 15.4 nm ± 3 nm at 12 s (with an outlier sample at 14 nm ± 4 nm at 6 s). The slope of the island-size increase is larger for a deposition potential of 0.47 V vs SHE than for 0.44 V vs SHE. Note that the height of the islands does not change with deposition duration; the sub-monolayer Cu UPD is always replaced by mono-atomically high Pd or Ir islands. The average Ir island size resulting from Cu deposition at 0.47 V vs SHE increases with increasing deposition duration from 10 nm ± 2 nm to a maximum of 31 nm ± 8 nm after 9 s and drops down to 13 nm ± 4 nm after 12 s of Cu UPD, and is thus larger than the corresponding Pd islands. It is known that Pd and Au interact strongly, sometimes

forming a (subsurface) alloy, while Ir is essentially not miscible with Au [33]. As such, Ir can be expected to possess a higher mobility on Au compared to Pd, which would favor the ad-atom growth into relatively larger islands. It would be exciting to study the island evolution by STM also on the atomic scale, ideally even at video rate. Such experiments, however, lie outside our current setup capabilities.

The results of the STM image analysis of Pd or Ir islands after Cu UPD displacement show that the average island size is larger for deposition at more positive potentials. This indicates that the deposition potential plays a role in the process of island formation. A lower deposition potential allows more nuclei to form than a more positive potential. Palomar-Pardavé et al. have shown that lower overpotentials require more Cu atoms to form a stable nucleus compared to higher overpotentials [25]. As such, a higher overpotential leads to a larger number of nuclei and, subsequently, of islands on the surface. In the growth phase following nucleation, the current density decays equally for both, high and low deposition potentials, following a $t^{-1/2}$ law (Fig. S35), *i.e.* the islands always grow in a way that is diffusion limited by the mass transport of Cu ions to the electrode. This observation is in accordance with results by Schmidt et al. [34]. In case of more negative deposition potentials where more islands form during nucleation, the islands, on average, grow smaller compared to more positive deposition potentials because of diffusion limitations while the total amount of Cu deposited after the nucleation is the same for both potentials.

The average inter-island distance also depends on the Cu UPD potential (SI Table S1). At a more negative deposition potential, more nuclei form, which leads to a distance between the islands that is smaller on average compared to the distances resulting from more positive deposition potentials. Pd islands resulting from Cu UPD with 6 s deposition duration at 0.47 V have an average inter-island spacing of 4.8 nm ± 3.5 nm whereas the same deposition duration at 0.44 V results in an inter-island spacing of only 1.5 nm ± 1.1 nm. The average inter-island spacing of Ir islands prepared under the same deposition conditions (0.47 V, 6 s) as Pd islands is found to be 12.1 nm ± 6.8 nm and thus significantly larger than for Pd.

These observations are in line with the results from complementary open circuit potential (OCP) measurements (Figs. S4–S13). OCP traces recorded during Pd galvanic displacement are affected by both, deposition potential and time, *i.e.* the Cu UPD coverage. A lower deposition potential and longer time, *i.e.* larger Cu islands, result in a ca. 12% relative larger OCP. No significant differences (<1%) were observed for Ir displacement.

Interestingly, the resulting Ir islands appear to be less uniform in their size distribution than the Pd islands with a standard deviation that is about twice as high as for Pd/Au(111). This observation can
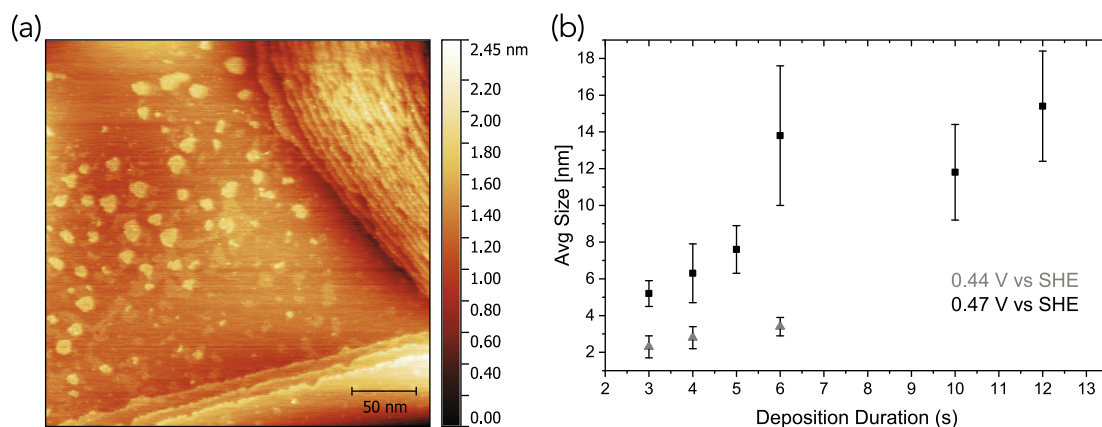
Fig. 3. (a) Example STM image of Au(111) surface after Pd displacement of Cu UPD (10 s UPD duration at 0.47 V vs SHE). (b) Correlation between the average size of Pd islands as obtained from STM image analysis and deposition duration of Cu UPD at different deposition potentials.
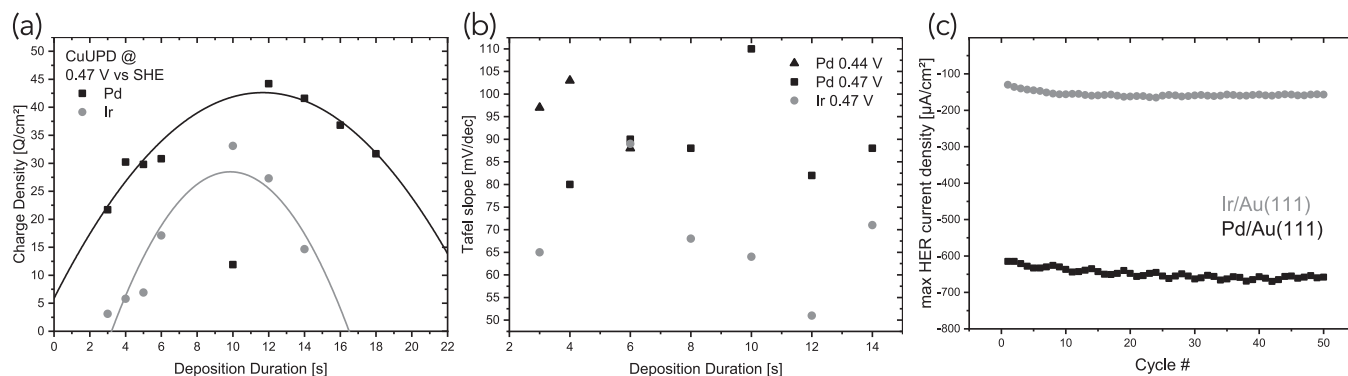
Fig. 4. a) HER activity of Pd and Ir 2D-confined islands as a function of Cu UPD deposition duration at 0.47 V vs SHE Cu UPD potential. b) Tafel slope as a function of deposition duration. c) Maximum HER charge density per cycle for Pd (black) and Ir (gray) islands recorded over 50 cycles.

be explained by considering the metal displacement reactions for the two metals as detailed below. The Pd displacement reaction employs a bivalent Pd salt (H_2PdCl_4) with an electron ratio to Cu of 1:1 when exchanged with Cu^{2+}:

$$H_2Pd^{II}Cl_4 + Cu^0 \rightarrow Pd^0_{(s)} + 4Cl^- + 2H^+ + Cu^{2+}_{(aq)} \qquad (1)$$

Ir, however, is used in form of its hydrochloride (H_2IrCl_6), containing an Ir atom with a charge of $+4$, *i.e.* two Cu atoms have to be oxidized for one Ir ion to be reduced according to the redox reaction:

$$H_2Ir^{IV}Cl_6 + 2Cu^0 \rightarrow Ir^0_{(s)} + 6Cl^- + 2H^+ + 2Cu^{2+}_{(aq)} \qquad (2)$$
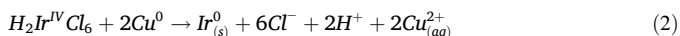
Consequently, Ir islands are separated into smaller agglomerations during the displacement process. Adatom diffusion can thus lead to differently sized islands with different inter-island distances, resulting in less uniform island formation compared to Pd islands on Au(1 1 1) that directly replace Cu UPD islands.

3.2. Effect of Cu UPD deposition duration, i.e. catalyst island size and distribution, on the HER activity

We evaluate the 2D islands with respect to their ability to catalyze the HER by analysing the transferred charge during the HER, the onset potential of the HER, *i.e.* the overpotential or cost of HER, and the Tafel slopes of the individual samples. A mass-activity optimized electro-catalyst surface should have largest possible current densities at low overpotentials with the least possible material employed. A Au (1 1 1) sample was used as reference sample. The samples were measured in a potential range from -0.2 V to 0.5 V vs SHE. HER onset potentials were obtained from CV measurements at scan rates of 25 mV/s to reduce the influence of diffusion limitation (Fig. S36).

The HER onset potential for the pristine a Au(1 1 1) surface was determined to be -0.13 V vs SHE under the given experimental conditions, about 110 mV more negative (or larger overpotential) than the value of -0.02 V vs SHE as observed at a rotating disc electrode [35,36]. The charge density obtained by integration between -0.13 V and -0.2 V vs SHE was found to be 1.67 $\mu C/cm^2$. The HER onset for catalyst islands on Au(1 1 1) was found to be -0.06 V vs SHE and -0.10 V vs SHE for Pd and Ir, respectively, independent of the island size. This finding shows that the overpotential for HER is independent of island size and inter-island spacing and only material dependent under the given conditions. The shift of $+70$ mV for the HER onset of Pd and of $+30$ mV on Ir/Au(1 1 1) compared to the one on Au(1 1 1) is in qualitative accordance with previous studies that report a more positive HER onset potential for Pd than for Ir (than for Au) [36].

A dependence of HER kinetics on the employed metal was found already in 1936 by Butler [37] and later explained by Trassati who related the exchange current density of the HER to the bond strength between adsorbed H atoms (H_{ads}) and catalyst metal in volcano plots [38,39]. The bond strength of Au-H_{ads} is too weak and the one of Ir-H_{ads} is too high for efficient HER catalysis; Pd exhibits a H_{ads} strength suitable for HER.

We find that the charge density of the HER strongly depends on the Cu UPD conditions and thus on the related 2D properties of the catalyst islands. Fig. 4a shows the correlation between HER charge density and Cu UPD deposition time at 0.47 V vs SHE for Pd/Au(1 1 1) (black) and Ir/Au(1 1 1) (gray) 2D catalyst surfaces. The HER charge increases for both, Pd and Ir islands up to a Cu UPD deposition time of 12 s and 10 s, corresponding to Pd and Ir islands of ca. 15 and 13 nm diameter and average inter-island distances of 5 and 10 nm, respectively. Here, maximum HER charge densities of 48 $\mu C/cm^2$ for Pd and 33 $\mu C/cm^2$ for Ir were obtained. For the highest ad-metal surface coverage of 0.32 ML (18 s and 14 s Cu UPD deposition duration at 0.47 V vs SHE for Pd and Ir islands, respectively), the HER activity drops again to reach charge densities of 33 $\mu C/cm^2$ for Pd and 14 $\mu C/cm^2$ for Ir islands. The data point at 10 s clearly is an outlier that is most likely caused by an unsuccessful Cu UPD as also indicated by the Tafel result (SI Fig. S37) that shows a significantly higher slope as expected for bare Au(1 1 1).

The decrease of HER activity for larger deposition times can be explained by a merging of the islands and thus a reduction of active sites with time (cf. STM images in Figs. S20–S26). A similar effect was reported before for Pd overlayers on Au(1 1 1) directly deposited from solution [9,11]. It has been repeatedly suggested that the primarily active sites of catalysts are defect sites such as step edge or kink sites [10,40,41]. A detailed theoretical study on HER on submonolayer Pd/Au(1 1 1) by Björketun et al. predicted a similar maximum HER exchange current density at intermediate Pd surface coverages, with hydrogen adsorption energies occurring at the rim of the Pd islands [14]. Note that the potential of zero charge of Pd has been found to be located at ca. 0.25 V vs RHE, independent of the Pd submonolayer coverage on Au(1 1 1) [42]. In our case, for short deposition times, the number of active edge sites increases as the circumference of the deposited islands grows. Apparently, with further island growth, the ad-atom diffusion path drops below a critical length that facilitates merging of islands. Island merging leads to a decrease in the number of catalytically active edge sites (at the Pd- or Ir-Au island rim) even when the overall catalyst surface coverage is increasing, and as a result, the HER activity drops.

Pd samples prepared at 0.44 V vs SHE Cu UPD potential up to 6 s deposition duration (maximum UPD coverage) led essentially always to approximate island sizes of 3 nm and inter-island distances of

2 nm, the smallest 2D confinement values investigated here. These fabrication conditions thus provided the highest average number of reactive edge sites for the given amount of Pd deposited and therefore the highest HER activities observed in this study between ca. 80 and 190 $\mu C/cm^2$ (Fig. S38). The HER activity should be a function of the total number of active sites of any given sample. Plotting the absolute boundary lengths as estimated from the STM images versus deposition time, we find a steady increase in rim length, with exception of the 5 s value, that correlates very well with the increase in HER activity (SI Fig. S39). The exceptional high density of small Pd islands in the 5 s deposition image might be explained by the fact that we are imaging close to a bunch of steps where Pd deposition might be favoured, in contrast to the other images recorded on wide terraces [43,44]. Note that the island edge length only gives a crude approximation of the number of active sites as it does not include defect or kink sites in/on the catalyst islands.

Comparing the Pd islands resulting from Cu UPD of 6 s at 0.47 V and at 0.44 V, we find a significant difference between the respective total boundary lengths and HER charge densities measured via CV (Table S1). The boundary length for 0.44 V is 3.17 μm while the one found at 0.47 V is 2.43 μm. The corresponding HER charge densities are 196.8 $\mu C/cm^2$ (0.44 V) and 30.8 $\mu C/cm^2$ (0.47 V). Assuming that during HER one electron is transferred per active Pd atom, the number of active atoms per unit area, n_{Pd}, are $1.23 \cdot 10^{21}$ atoms/cm^2 (0.44 V, 6 s) and $1.93 \cdot 10^{20}$ atoms/cm^2 (0.47 V, 6 s). If we further assume that only Pd edge atoms are active catalysts for HER, n_{Pd} is the number of edge atoms per unit area. From STM image analysis and the measured boundary lengths, we can estimate the approximate number of active edge atoms to be $6.68 \cdot 10^{13}$ atoms/cm^2 (0.44 V) and $3.01 \cdot 10^{13}$ atoms/cm^2 (0.47 V), which is much less than the number calculated from the measured charge densities but in qualitative agreement. As stated above, the STM image analysis shows a large variation and is not quantitatively comparable to the HER analysis.

The Tafel slopes as extracted from the polarization curves in Figs. S37, S40 and S41 (not corrected for the iR drop) range between 80 and 90 mV/dec for Pd after Cu UPD@0.47 V (Fig. 4b). The outlier at 10 s deposition time is likely caused by an unsuccessful Pd deposition and thus exhibits a Tafel slope of 110 mV/dec as expected for bare Au(111), in line with the low HER charge density. For Pd after Cu UPD@0.44 V, the Tafel slopes are slightly larger between 88 and 103 mV/dec. Tafel slopes of around 70 mV/dec have been reported for spontaneously deposited Pd submonolayers on Au(111) [11]. For the Ir island samples, we obtain values between 51 and 89 mV/dec, which is a range comparable to the 60 mV/dec previously reported [45].

Generally, the Tafel slope is used to determine the rate determining step of the HER. A pristine Au(111) surface shows a Tafel slope of 110 mV/dec, assigned to a Volmer-Heyrovsky Mechanism [11]. The Volmer-Heyrovsky Mechanism for HER is characterized by a Volmer step that describes the adsorption and reduction of hydrogen atoms resulting in a MH_{ads} species, followed by a subsequent, rate determining Heyrovsky step, $MH_{ads} + H^+ + e^- \rightleftharpoons M + H_2$ [46].

The Pd and Ir samples show significant lower Tafel slopes of 80–90 mV/dec and 50–90 mV/dec, respectively. Low Tafel slopes indicate lateral interactions between the surface atoms and adsorbed hydrogen [11] so that no H^+ from the electrolyte is needed to produce H_2 like in a Heyrovsky step, but instead, the reaction occurs by a Tafel step: $MH_{ads} + MH_{ads} \rightleftharpoons 2M + H_2$ [46]. Values of 60 mV/dec as found for Ir/Au(111) can therefore be assigned to a Volmer-Tafel Mechanism with a rate determining Tafel step. The slightly higher values of the Pd/Au(111) samples indicate Volmer-Heyrovsky sequences with slow Volmer steps, as was also reported by Smiljanic et al. for a Pd/Au(111) system [11]. While the variations in Tafel slopes between individual samples of Pd are small in the order of 10%, indicating that changes in the island morphology do not greatly affect the HER mechanism,

smaller islands seem to tend toward Volmer-Heyrovsky reaction sequences [11].

To obtain a more detailed understanding of sample-dependent HER mechanism and kinetics, high-resolution STM images and nanoscale spectroscopy, which could shed light on Pd and Au atomic locations, chemical interactions and dynamics, would be helpful, but lie beyond the scope of this technical paper.

3.3. 2D catalyst stability

One important aspect for the development of improved electro-catalyst surfaces is their stability during operation. We have tested the long-term stability of the 2D Pd and Ir islands on Au(111) with CV in the potential range between -0.2 V vs SHE and 0.5 V vs SHE in 50 cycles (Fig. 4c). The charge density in the HER potential region can be used as an indicator for the presence of Pd or Ir reactive sites. The HER charge density exhibits only small losses in the order of $<1\%$ for Pd and 5% for Ir over time, indicating that the catalyst islands are stable in this potential range.

We also examined the stability of the 2D-confined catalyst layers in a wider potential range to assess the maximum potential window accessible for use in electrochemical reactions in aqueous solutions. CVs were recorded with a varying upper potential limit between 0.6 and 1 V vs SHE where surface oxidation starts to play a crucial role and can cause deactivation of the catalyst. The data shows that loss of catalytic activity starts at around 0.75 V vs SHE for Pd islands (Fig. S42). The potential where the loss of catalytic activity starts for our samples is slightly lower than the onset potential of Pd defect oxidation at ca. 0.844 V vs SHE as reported by Kolb et al. [9], in line with under-coordinated, highly reactive edge sites on the 2D-confined Pd catalysts. Oxidation of the nanoscale Pd islands can be expected to lead to dissolution of the sub-monolayer deposit and therefore to a degradation of the electro-catalytic activity of the sample [47]. Since the oxidation of defect (kink, step) sites is thermodynamically more favorable than the oxidation of terrace structures, island oxidation occurs first at the island/Au boundary [47], which leads to an immediate inhibition of HER active sites. The thermodynamics of surface oxidation suggests that the onset potential for island degradation is influenced by the size distribution of the islands. For a large number of small islands, the ratio of rim-to-terrace sites is higher and sample degradation occurs faster than for fewer, larger islands because of the lower oxidation overpotential for terrace sites compared to defect sites.

4. Summary

To summarize, in this work, we have presented a simple route toward fabrication of 2D-confined Pd and Ir catalyst islands of controllable size and inter-island distance on Au(111). The catalyst island size and surface distribution is controlled by tuning the potential and duration of Cu UPD and subsequent galvanic displacement of the resulting Cu islands by Pd or Ir.

We find that at lower deposition potential, smaller islands of 2–3 nm average diameter form while a higher deposition potential leads to a larger size distribution varying between 5 and 14 nm that can be tuned with help of the deposition duration. The potential-dependent size is a result of the potential-dependent number of Cu nuclei being formed prior to metal displacement. The average catalyst inter-island distance remains at around 1.5 nm at lower deposition potential, while for higher deposition potential, the spacing increases to on average 4.8 nm for Pd and 12.1 nm for Ir. This difference can be explained through the Cu-to-metal exchange ratio that amounts to 1:1 for Cu $\rightarrow$ Pd and to 2:1 for Cu $\rightarrow$ Ir because of the different valence states of the salts employed for galvanic displacement.

Characterizing the different samples in terms of their catalytic activity, we find that the HER activity varies as a function of

deposition time at 0.47 V vs SHE. Here, our data thus suggests an optimal combination of 2D catalyst confinement with an island size of 13–14 nm and an inter-island spacing of 5 nm for Pd and 10 nm for Ir catalyst sub-monolayers that can be reached with deposition durations of 10–12 s. Catalyst islands fabricated from Cu UPD at low potential (0.44 V vs SHE), *i.e.* catalysts that are confined to around 2 nm size, exhibit a factor 3–4 stronger HER activity than the slightly larger islands obtained following Cu UPD at 0.47 V vs SHE. The long-term stability of the 2D catalysts is characterized by small drops in HER activity of up to 5% in the potential range up to 0.5 V vs SHE, but is significantly reduced at potentials above 0.75 V due to the early onset of PGM oxidation at reactive sites.

To conclude, our work provides a strategic fabrication route for 2D-confined Pd or Ir catalyst islands that are highly active for HER. With this approach, high-active mass catalyst surfaces can be fabricated in a controlled, tunable fashion. Such well-defined PMG islands are excellent samples to explore the fundamentals of catalytic mechanisms and electrode surface (re)activities.

CRediT authorship contribution statement

Daniel Ohm: Conceptualization, Methodology, Investigation, Formal analysis, Validation, Data curation, Writing - original draft, Visualization. **Katrin F. Domke:** Conceptualization, Methodology, Resources, Data curation, Validation, Project administration, Writing - review & editing, Funding acquisition, Supervision.

Declaration of Competing Interest

The authors declare that they have no known competing financial interests or personal relationships that could have appeared to influence the work reported in this paper.

Acknowledgements

Appendix A. Supplementary data

Supplementary data to this article can be found online at https://doi.org/10.1016/j.jelechem.2021.115285.

References

[1] Y. Cheng, S.P. Jiang, Pro. Nat. Sci. Mater. 25 (2015) 545–553.
[2] D.V. Esposito, J.G. Chen, Energy Environ. Sci. 4 (2011) 3900–3912.
[3] C. Rakousky, G.P. Keeley, K. Wippermann, M. Carmo, D. Stolten, Electrochim. Acta 278 (2018) 324–331.
[4] J.C.C. Gómez, R. Moliner, M.J. Lázaro, Catalysts 6 (2016) 130–150.
[5] D.V. Esposito, S.T. Hunt, Y.C. Kimmel, J.G. Chen, J. Am. Chem. Soc. 134 (2012) 3025–3033.
[6] M. Li, Z. Zhao, et al, Science 354 (2016) 1414–1419.
[7] S. Sarkar, S.C. Peter, Inorg. Chem. Front. 5 (2018) 2060–2080.
[8] L.A. Kibler, M. Kleinert, R. Randler, D.M. Kolb, Surf. Sci. 443 (1999) 19–30.
[9] J. Tang, M. Petri, L.A. Kibler, D.M. Kolb, Electrochim. Acta 51 (2005) 125–132.
[10] F. Hernandez, H. Baltruschat, J. Sol. State Electrochem. 11 (2007) 877–885.
[11] M. Smiljanić, I. Srejić, B. Grgur, Z. Rakočević, S. Štrbac, Electrocatalysis 3 (2012) 369–375.
[12] G.A.B. Mello, C. Busó-Rogero, E. Herrero, J.M. Feliu, J. Chem. Phys. 150 (2019) 041703.
[13] S. Pandelov, U. Stimming, Electrochim. Acta 52 (2007) 5548–5555.
[14] M.E. Björketun, G.S. Karlberg, J. Rossmeisl, I. Chorkendorff, H. Wolfschmidt, U. Stimming, J.K. Nørskov, Phys. Rev. B 84 (2011) 045407.
[15] S.R. Brankovic, J.X. Wang, R.R. Adžić, Surf. Sci. 474 (2001) L173–L179.
[16] O.M. Magnussen, J. Hotlos, R.J. Nichols, D.M. Kolb, R.J. Behm, J. Phys. Rev. Lett. 64 (1990) 2929.
[17] J. Hotlos, O.M. Magnussen, R.J. Behm, Surf. Sci. 335 (1995) 129–144.
[18] E. Herrero, L.J. Buller, H.D. Abruña, Chem. Rev. 101 (2001) 1897–1930.
[19] E. Herrero, S. Glazier, L.J. Buller, H.D. Abruña, J. Electroanal. Chem. Rev. 461 (1999) 121–130.
[20] H. Uchida, M. Hiei, M. Watanabe, J. Electroanal. Chem. 452 (1998) 97–106.
[21] Z. Shi, J. Lipkowski, S. Mirwald, B. Pettinger, J. Electroanal. Chem. 396 (1995) 115–124.
[22] T. Hachiya, H. Hombi, K. Itaya, J. Electroanal. Chem. 315 (1991) 275–291.
[23] M.S. Zei, G. Qiao, G. Lehmpfuhl, D.M. Kolb, Phys. Chem. 91 (1987) 349.
[24] J. Hotlos, O.M. Magnussen, R.J. Behm, Surf. Sci. 311 (1994) L641.
[25] M. Palomar-Pardavé, I. González, N. Batina, J. Phys. Chem. B 15 (2000) 104.
[26] J.G. Xu, X.W. Wang, Surf. Sci. 408 (1998) 317–325.
[27] M.H. Hölzle, U. Retter, D.M. Kolb, J. Electroanal. Chem. 371 (1994) 101–109.
[28] E. Garfias-Garcia, M. Palomar-Pardavé, M. Romero-Romoc, M.T. Ramírez-Silvad, N. Batinae, ECS Trans. 3 (2007) 35–43.
[29] N. Mayet, K. Servat, K.B. Kokoh, T.W. Napporn, Surfaces 2 (2019) 257–276.
[30] A. Kuzume, E. Herrero, J.M. Feliu, R.J. Nichols, D.J. Schiffrin, Phys. Chem. Chem. Phys. 6 (2004) 619–625.
[31] T. Hashîya, H. Honbo, K. Itava, J. Electroanal. Chem. 315 (1991) 275–291.
[32] V. Mehar, C.R. O'Connor, T. Egle, M. Karatok, R.J. Madix, C.M. Friend, J.F. Weaver, Phys. Chem. Chem. Phys. 22 (2020) 6202–6209.
[33] J. Gong, Chem. Rev. 112 (2012) 2987–3054.
[34] E. Schmidt, W.S. Lorenz, K. Jüttner, G. Statkov, Electrochim. Acta 23 (1978) 305–313.
[35] D. Strmcnik, M. Uchimura, C. Wang, et al, Nat. Chem. 5 (2013) 300–306.
[36] H. Angerstein-Kozlowska, B.E. Conway, A. Hamelin, J. Electroanal. Chem. 277 (1990) 233–252.
[37] J.A.V. Butler, Proc. R. Soc. Lond. A157 (1936) 423–433.
[38] S. Trasatti, J. Electroanal. Chem. 39 (1972) 163–184.
[39] O.A. Petrii, G.A. Tsirlina, Electrochim. Acta 39 (1994) 1739.
[40] R. van Lent et al, Science 363 (2019) 155–157.
[41] J. Fester et al, Angew. Chem. Intl. Ed. 57 (2018) 11893–11897.
[42] B. Álvarez, V. Climent, J.M. Feliu, A. Aldaz, Electrochem. Comm. 2 (2000) 427–430.
[43] R.J. Nichols, D.M. Kolb, R.J. Brehm, J. Electroanal. Chem. Interface Electrochem. 313 (1991) 109–119.
[44] N. Batina, T. Will, D.M. Kolb, Faraday Discuss. 94 (1992) 93–106.
[45] S. Štrbac, I. Srejić, Z. Rakočević, J. Electrochem. Soc. 165 (2018) J3335–J3341.
[46] M. Bhardwaj, R. Balasubramaniam, J. Hydrog, Energy 33 (2008) 2178–2188.
[47] A.M. El-Aziz, L.A. Kibler, J. Electroanal. Chem. 534 (2002) 107–114.